Croatian Society for Materials Protection

Distribution Influence of Functional Gradient Graphene Reinforced Composites in Solving Differential Equations

Duanyin Shi and Chunyan Zhao*

College of Science, Heilongjiang University of Science and Technology, Harbin150022, China
*Correspondence: Zhaochunyan0217@126.com

Abstract: To investigate the effects of different graphene block distribution modes on the vibration characteristics of functionally graded graphene-reinforced composite materials, this study first establishes the motion control differential equations based on the Halpin–Tsai micromechanical model and Hamilton's principle. The nonlinear and free vibration behaviors of the materials are also analyzed. The results indicate that different graphene mass fractions and distribution patterns have varying degrees of influence on the resonance characteristics and mechanical properties of functionally graded graphene layer–reinforced composites. Among them, the cross distribution pattern exhibits the most effective vibration suppression under specific conditions. These findings provide a theoretical foundation for the development of lightweight, high-strength materials and contribute to understanding the inherent relationship between the distribution of graphene blocks and material properties.

1. Introduction

The need for high-performance composite materials has become increasingly pressing as science and technology continue to advance at an accelerated rate. These composites must exhibit not only excellent mechanical properties but also effective vibration control capabilities [1]. As a rapidly developing class of materials, functionally graded materials (FGMs), with their unique performance gradient design, offer a promising solution to these requirements [2]. Functionally graded graphene-reinforced composite materials (FG-GPLRCs) represent a novel type of composite in which graphene is incorporated as reinforcement through specific spatial distribution patterns [3]. By combining the advantages of FGMs with the exceptional stiffness and strength of graphene, these materials achieve significant improvements in mechanical performance due to their graded or uniformly distributed structure through the thickness.

Graphene, owing to its extremely high specific surface area and modulus, serves as an effective reinforcing phase that can substantially enhance the stiffness and strength of composite matrices. For instance, extensive reactive molecular dynamics simulations have shown that graphene-reinforced composites possess considerably higher tensile modulus and strength compared with graphene-free systems [4]. To improve graphene oxide's mechanical efficiency, a deep reinforcement learning–based design strategy has also been proposed, resulting in graphene oxide structures whose toughness exceeds that of randomly generated configurations by more than two standard deviations [5].

Further studies have examined the static response of functionally graded porous nanocomposite beams using a combination of nonlocal strain gradient theory and finite element analysis, demonstrating that graphene sheet distribution patterns and porosity significantly influence structural performance [6]. Analytical approaches have also been used to identify optimal elastic foundation distributions, showing that simplified refined plate theories adequately capture the relationship between FG-GPLRC properties and displacement fields [7]. Additional research has shown that functionally graded structures, in which the weight fraction of graphene nanosheets varies smoothly along the thickness of disk-axis rotors, can be effectively modeled using Lagrangian equations that incorporate gyroscopic effects [8]. Electromechanical studies employing a modified Halpin–Tsai model have indicated that the material grading index substantially affects the electrical characteristics of FG-GPLRCs [9].

While previous work has provided valuable insights into the static mechanical performance of FG-GPLRCs, their dynamic behavior—particularly nonlinear and free vibration (FV) characteristics—remains insufficiently explored. Differential equations (DEs), as fundamental tools for describing mechanical behavior, offer considerable potential for advancing research in this area [10]. Recent developments include neural-network-based solvers that combine orthogonal polynomials with physics-informed methods to efficiently address nonlinear partial differential equations [11]. Other investigations have used DE-based models to assess how nano-reinforcements influence the elastic characteristics of FGMs, confirming substantial improvements in material behavior when reinforcement units are included [12]. Approximate solutions for fractional differential equations have also been obtained using the Mohand transform and fractional complex transformations, simplifying numerical simulation procedures [13]. Additionally, fourth-order time-fractional partial differential equations have been analyzed using polynomial-based discriminant systems, enabling the determination of exact dynamic characteristics such as phase diagrams [14].

Studies on the buckling and post-buckling behavior of FG-GPLRCs under external electric fields have shown that the stability of graphene-reinforced composite plates can be tailored by adjusting electric-field parameters, with governing equations solved using differential quadrature methods [15]. Furthermore, research on nanofluids and enhanced oil recovery has demonstrated that thermophysical behavior can be reduced to nonlinear differential equations via similarity transformations, with approximate solutions obtained using Chebyshev collocation methods [16].

In summary, substantial progress has been made in enhancing the strength, toughness, and static response of graphene-based composites. However, the vibrational behavior of FG-GPLRCs—particularly their nonlinear and free vibration characteristics—remains insufficiently understood, and their dynamic mechanical properties have yet to be comprehensively investigated. Therefore, this study develops motion-control differential equations for FG-GPLRCs using the Halpin–Tsai micromechanical model (HTMM) and Hamilton's principle (HP). The aim is to provide a deeper understanding of their nonlinear and FV behavior through theoretical modeling and numerical analysis, thereby offering a scientific basis for performance optimization and structural design in engineering applications. The novelty of the present work lies in formulating the governing motion equations by integrating the HTMM, first-order shear deformation theory (1st-SDT), and HP.

2. Materials and Methods

To investigate how different graphene block distributions influence the characteristics of FG-GPLRCs, the study first establishes the motion-control DEs based on the HTMM and HP. This is followed by a nonlinear mechanical analysis, after which the free-vibration behavior of the FG-GPLRC is examined.

2.1. Kinetic Equation Building and Nonlinear Mechanical Analysis of FG-GPLRC

The study first develops the kinetic equations to shed light on the relationship between the governing equations of motion and the mechanical characteristics of the material, thereby establishing a theoretical framework for further analysis. The FG-GPLRC is modeled as a rectangular plate structure. It consists of graphene-reinforced composite layers of equal thickness, with each layer strengthened by graphene blocks serv-

ing as the reinforcing phase. The length, width, and height of the FG-GPLRC are denoted by a, b, and h, respectively, and the total number of layers is N. The four graphene block distribution patterns are shown in Figure 1.

(a) U-GPLRC   (b) X-GPLRC

(c) O-GPLRC   (d) A-GPLRC
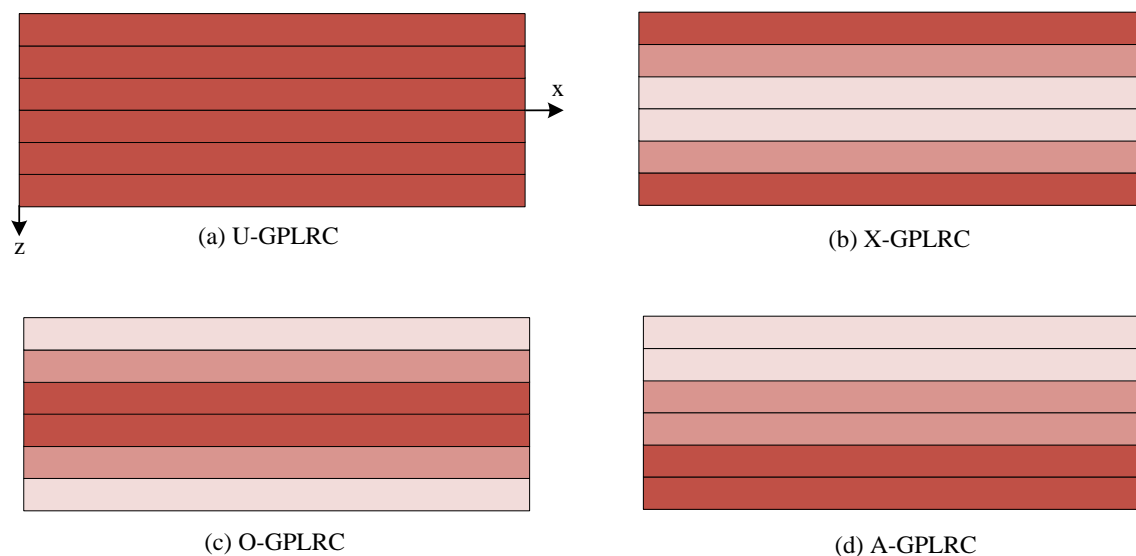
Figure 1. Four distribution patterns of graphene blocks

In Figure 1, the darker color indicates a higher content of graphene reinforcement. The mass fraction (MF) of graphene varies gradually with the number of layers, and each graphene layer is assumed to be isotropic in the x-axis direction. In the Uniform-GPLRC (U-GPLRC), all layers contain the same amount of graphene, uniformly distributed throughout the matrix. In the Cross-GPLRC (X-GPLRC), the graphene content is highest in the surface layer and lowest in the middle layer. The Optimal-GPLRC (O-GPLRC) exhibits the opposite distribution, with graphene concentrated in the middle layer. In the Adversarial-GPLRC (A-GPLRC), the graphene content increases progressively from the upper to the lower surface. The approximate expression for the Young's modulus (YM), E, of the composite is given in Equation (1) [17].

$$E = \frac{3}{8}E_L + \frac{5}{8}E_r \tag{1}$$

In Equation (1), E_L and E_r denote the longitudinal and transverse moduli of unidirectional laminates, respectively. The HTMM was developed for evaluating the stiffness and swelling behavior of oriented short-fiber composites [18]. In this study, the Young's modulus E of each graphene-flake-reinforced layer is estimated using the HTMM, as shown in Equation (2) [18].

$$\begin{cases} E = \frac{3+3\varpi_L\eta_L V_G E_m}{8(1-\eta_L V_G)} + \frac{5+5\varpi_T\eta_T V_G E_m}{8(1-\eta_L V_G)} \\ \eta_L = \frac{(E_G/E_m)-1}{(E_G/E_m)-\varpi_L} \\ \eta_T = \frac{(E_G/E_m)-1}{(E_G/E_m)-\varpi_T} \end{cases} \tag{2}$$

In Equation (2), E_G and E_m denote the Young's moduli of the graphene flakes and composites, respectively. V_G represents the volume fraction (VF) of graphene flakes. η_L and η_T denote the geometrical parameters of graphene flakes in the longitudinal and transverse directions, respectively, while ϖ_L and ϖ_T represent corresponding geometrical parameters of the graphene material. The effective Young's modulus of the FG-GPLRC for different graphene block distribution modes is shown in Figure 2.
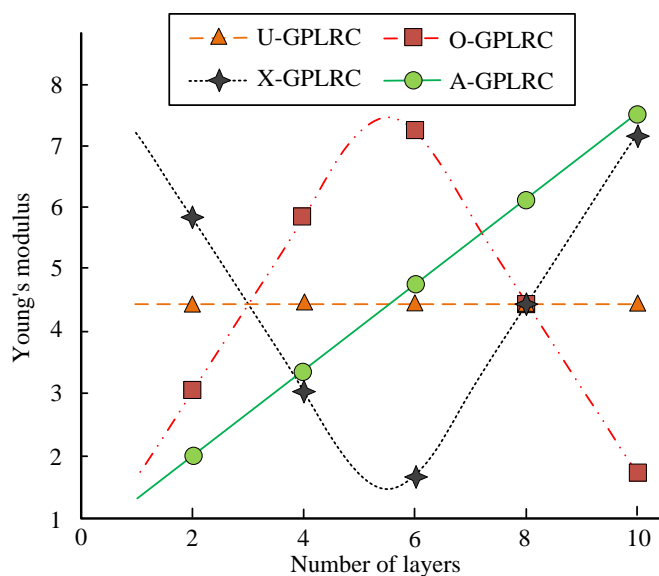
Figure 2. YM of FG-GPLRC under different distribution modes

In Figure 2, the higher the content of graphene reinforcement, the higher the effective YM of the layer. According to the mixing criterion, the Poisson's ratio (PR) v and mass density (MD) ρ of each layer are calculated as shown in Equation (3) [19].

$$\begin{cases} v = v_G V_G + v_m V_m \\ \rho = \rho_G V_G + \rho_m V_m \end{cases} \tag{3}$$

In Equation (3), v_G and v_m denote the PR of graphene flakes and composites respectively . ρ_G and ρ_m denote the MDs of graphene flakes and composites, respectively. V_m is the VF of the composite. The 1st-SDT can more accurately describe the MB of medium-thickness structures and is specially suitable for engineering problems that consider the influence of transverse shear effects [20]. Therefore, it is used to construct the nonlinear dynamic equations of FG-GPLRC. According to the 1st-SDT, the displacement field (DF) of FG-GPLRC is shown in Equation (4) [20].

$$\begin{cases} U(X,Y,Z,t) = u(X,Y,t) + Z \frac{\partial U}{\partial Z}(X,Y,t) \\ V(X,Y,Z,t) = v(X,Y,t) + Z \frac{\partial U}{\partial Z}(X,Y,t) \\ \qquad W(X,Y,Z,t) = w(X,Y,t) \end{cases} \tag{4}$$

In Equation (4), t denotes time. $u(X,Y,t)$, $v(X,Y,t)$, and $w(X,Y,t)$ denote the mid-plane displacement components of the FG-GPLRC. Figure 3 shows the schematic diagram of the 1st-SDT.
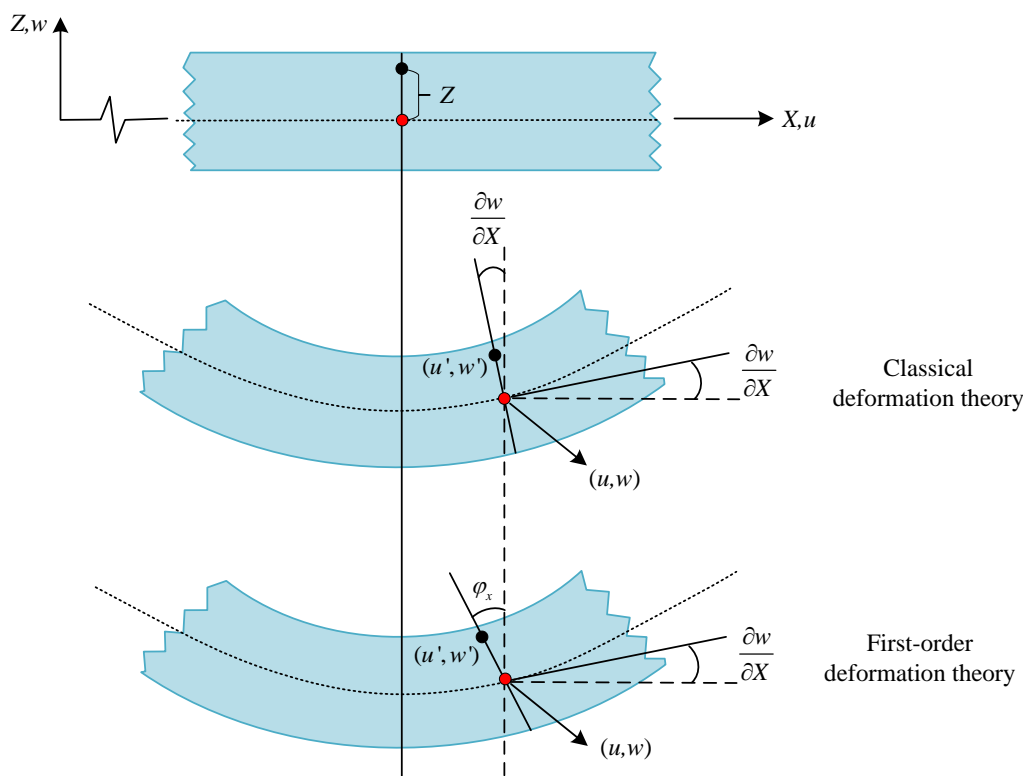
Figure 3. Schematic diagram of 1st-SDT

In Figure 3, the classical deformation theory assumes that the normal after deformation is still perpendicular to the midplane and of constant length. The 1st-SDT assumes that the normal is straight and of constant length after deformation, but allows it to tilt while maintaining its length. The difference between the two theories lies in whether or not shear deformation is considered. Classical theory ignores shear deformation and is applicable to thin plate analysis. First-order theory, on the other hand, considers shear deformation and is applicable to thick plates or situations where shear deformation is significant. Equation (5) illustrates the nonlinear strain-displacement relationship of FG-GPLRC in accordance with the von Karmen geometric nonlinearity principle [21].

$$\begin{cases} \varepsilon_{xx} = \frac{\partial u}{\partial X} + z\frac{\partial \varphi}{\partial X} + \frac{1}{2}(\frac{\partial w}{\partial X})^2 \\ \gamma_{xz} = \frac{\partial w}{\partial X} + \varphi \end{cases} \tag{5}$$

In Equation (5), ε_{xx} denotes the strain component. φ denotes the angle of rotation of the cross-section at any point on the neutral axis. w and u denote the displacements along the Z-axis and X-axis directions. After obtaining the nonlinear strain displacement relationship shown in equation (5), the normal stress and shear stress at any point in FG-GPLRC can be determined based on the constitutive relationship, as shown in Equation (6) [21].

$$\begin{cases} \sigma_{xx} = Q_{11}(Z)\varepsilon_{xx} \\ \sigma_{xz} = kQ_{55}(Z)\gamma_{xz} \end{cases} \tag{6}$$

In Equation (6), $Q_{11}(Z)$ and $Q_{55}(Z)$ denote the degenerate stiffnesses. k denotes the shear correction factor. HP utilizes the variational method to describe the laws of motion of a mechanical system and is commonly used to model the dynamics of systems with continuous mass and stiffness distributions [22]. According to HP, the NDE of motion of FG-GPLRC under dynamic loading is given in Equation (7) [22].

$$\begin{cases} \frac{\partial F_{xx}}{\partial X} + \frac{\partial F_{xy}}{\partial Y} = I_0 \frac{\partial^2 u}{\partial t^2} + I_1 \frac{\partial^2 \varphi_x}{\partial t^2} \\ \frac{\partial F_{xy}}{\partial X} + \frac{\partial F_{yy}}{\partial Y} = I_0 \frac{\partial^2 v}{\partial t^2} + I_1 \frac{\partial^2 \varphi_y}{\partial t^2} \\ \frac{\partial M_{xx}}{\partial X} + \frac{\partial F_{xy}}{\partial Y} - C_x = I_2 \frac{\partial^2 \varphi_x}{\partial t^2} + I_1 \frac{\partial^2 u}{\partial t^2} \\ \frac{\partial M_{xy}}{\partial X} + \frac{\partial F_{yy}}{\partial Y} - C_y = I_2 \frac{\partial^2 \varphi_y}{\partial t^2} + I_1 \frac{\partial^2 v}{\partial t^2} \\ \frac{\partial C_x}{\partial X} + \frac{\partial C_y}{\partial Y} + \Delta(w) + F(X,Y,t) - \mu \frac{\partial w}{\partial t} = I_0 \frac{\partial^2 w}{\partial t^2} \end{cases} \quad (7)$$

In Equation (7), I_i denotes the inertia term. $F(X,Y,t)$ denotes the dynamic load. φ_x and φ_y are the rotations of the cross-section about the x and y axes. C_x and C_y denote shear forces. F_{xx}, F_{xy}, and F_{yy} denote axial forces. M_{xx}, M_{xy}, and M_{yy} denote bending moments. After constructing the NDEs of motion of the FG-GPLRC, the nonlinear MB of the FG-GPLRC is further analyzed. Galyokin's method is applied to discretize the set of NDEs of motion of the FG-GPLRC. Equation (8) defines the non-dimensional displacements in order to meet the simply supported boundary conditions [23].

$$\begin{cases} u' = \frac{u}{h} = \sum_{m-1}^{M} \sum_{f-1}^{F} u(t) \cos \quad m\pi \frac{X}{a} \sin \quad n\pi \frac{Y}{b} \\ w' = \frac{w}{h} = \sum_{m-1}^{M} \sum_{f-1}^{F} w(t) \sin \quad m\pi \frac{X}{a} \sin \quad n\pi \frac{Y}{b} \\ v' = \frac{v}{h} = \sum_{m-1}^{M} \sum_{f-1}^{F} v(t) \sin \quad m\pi \frac{X}{a} \cos \quad n\pi \frac{Y}{b} \\ \varphi_x = \sum_{m-1}^{M} \sum_{f-1}^{F} \varphi(t) \cos \quad m\pi \frac{X}{a} \sin \quad n\pi \frac{Y}{b} \\ \varphi_y = \sum_{m-1}^{M} \sum_{f-1}^{F} \varphi(t) \sin \quad m\pi \frac{X}{a} \cos \quad n\pi \frac{Y}{b} \end{cases} \quad (8)$$

In Equation (8), v denotes the displacement along the y-axis. $u(t)$, $w(t)$, $v(t)$, $\varphi(t)$ denote the unknown functions of non-dimensional time *t*. To simplify the calculation, the study ignores u, v, v, and φ_y when constructing the differential control equations for the nonlinear motion of the FG-GPLRC. The final differential control equations obtained are shown in Equation (9).

$$\begin{cases} \ddot{w}_1 + \zeta_1 \dot{w}_1 + \omega_1^2 w_1 + K_1 w_1^3 + K_2 w_1 w_2^2 = \vartheta_1 \kappa \ \cos(\Omega_1 t) \\ \ddot{w}_2 + \zeta_2 \dot{w}_2 + \omega_2^2 w_2 + K_3 w_2^3 + K_4 w_2 w_1^2 = \vartheta_2 \kappa \ \cos(\Omega_2 t) \end{cases} \quad (9)$$

In Equation (9), K is the stiffness coefficient. ϑ is the external excitation coefficient. ζ denotes the damping coefficient. κ denotes the external excitation divided by E_m. Ω_1 and Ω_2 represent the angular frequencies of the external excitations in two different modes.

2.2. FV Analysis of FG-GPLRC

The study analyzes the nonlinear MB of FG-GPLRC, but understanding its nonlinear properties alone is not sufficient to comprehensively assess the dynamic performance of the material in practical applications. Therefore, to further understand how well FG-GPLRC performs in vibration situations and to provide as a foundation for material design and optimization, the study also examines its FV behavior. FV is the term used to describe a system's vibration when no external stimulation is present. The inherent features of the system dictate its frequency, also known as the intrinsic frequency. FV happens following an initial disturbance to a system. In the presence of damping and in the absence of a continuous external force, the vibration's amplitude progressively decreases over time. Figure 4 displays the FG-GPLRC schematic diagram on an elastic basis.
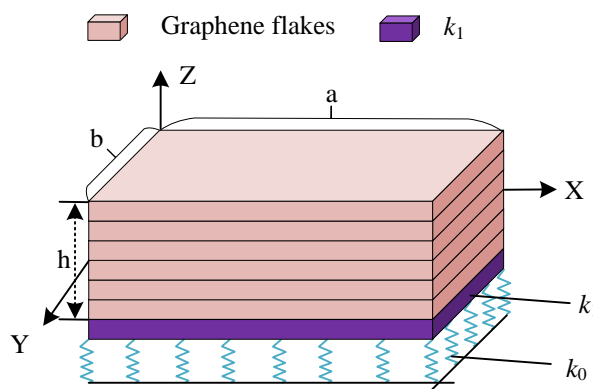
Figure 4. Schematic diagram of FG-GPLRC on EF

Elastic foundation (EF) is added beneath the FG-GPLRC matrix in Figure 4, but the physical characteristics of the matrix remain the same as in the nonlinear mechanical analysis section. The Pasternak foundation (PF) model and the Hetenyi model are two common two-parameter models. The Hetenyi model is based on the Winkler model and introduces an elastic plate or elastic beam with a flexural stiffness DDD to simulate the interaction between the independent spring units. The Winkler model assumes that the foundation consists of a series of independent springs [24]. Each spring's deformation is independent of the others, although it is proportional to the force applied to it. As a result, it fails to capture the continuity of the foundation soil and the action of shear stress. To address the limitations of the Winkler model in characterizing the continuous nature of real soil, the PF model was developed based on it [25]. Compared with the Hetenyi model, the PF model has a clearer physical meaning and performs better under different boundary conditions. Therefore, the PF model is used in this study. The EF consists of a Winkler foundation with elastic stiffness parameter k0k_0k0 and a PF shear layer with shear stiffness parameter k1k_1k1. The schematic diagram of the Pasternak and Hetenyi foundation models is shown in Figure 5.
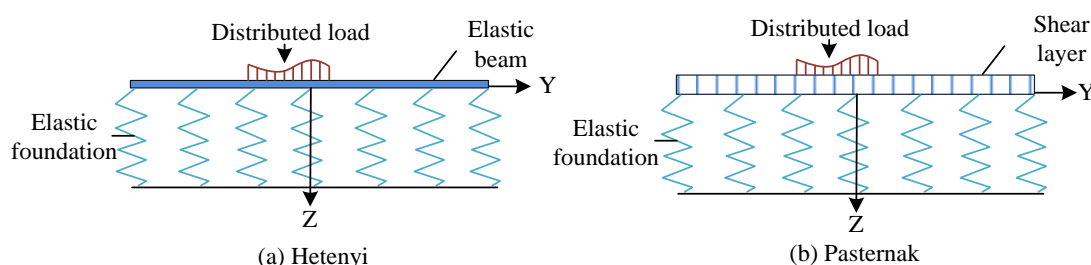
Figure 5. Schematic diagram of Pasternak and Hetenyi foundation models

In Figure 5, the Hetenyi model consists of an elastic beam and an EF, and is mainly used to analyze the combined action of the beam and the foundation. The PF model consists of an EF and a shear layer, and is able to account for both the vertical stiffness and the horizontal shear stiffness of the foundation. Higher-order shear refinement plate theory (HO-SRPT) is a method used to analyze laminated composite structures. Legendre polynomials are used to approximate the distribution of the DF along the thickness direction, which allows this method to better capture the transverse shear effect and interlaminar deformation. To more accurately analyze the FV characteristics of the FG-GPLRC, this study uses HO-SRPT to construct the model. The DF of the FG-GPLRC with a rectangular plate structure is shown in Equation (10) [26].

$$\begin{cases} u' = u - Z\frac{\partial w_b}{\partial X} - \left(-\frac{Z}{4} + \frac{5Z^3}{3h^2}\right)\frac{\partial w_s}{\partial X} \\ v' = v - Z\frac{\partial w_b}{\partial Y} - \left(-\frac{Z}{4} + \frac{5Z^3}{3h^2}\right)\frac{\partial w_s}{\partial Y} \\ w = w_b + w_s \end{cases} \tag{10}$$

In Equation (10), w_b is the bending portion of the lateral displacement. w_s is the shear portion of the transverse displacement. The strain components in each direction are shown in Equation (11) [26].

$$\begin{cases} \varepsilon_{xx} = \frac{\partial u}{\partial X} + z\frac{\partial^2 w_b}{\partial X^2} + \left(\frac{5Z^3}{3h^2} - \frac{Z}{4}\right)\frac{\partial^2 w_s}{\partial X^2} \\ \varepsilon_{yy} = \frac{\partial v}{\partial Y} + z\frac{\partial^2 w_b}{\partial Y^2} + \left(\frac{5Z^3}{3h^2} - \frac{Z}{4}\right)\frac{\partial^2 w_s}{\partial Y^2} \\ \varepsilon_{xy} = \frac{\partial v}{\partial Y} + \frac{\partial v}{\partial X} + 2z\frac{\partial^2 w_b}{\partial X\partial Y} + 2\left(\frac{5Z^3}{3h^2} - \frac{Z}{4}\right)\frac{\partial^2 w_s}{\partial X\partial Y} \end{cases} \tag{11}$$

The relationship between a material's stress and strain within the range of elastic deformation is described by generalized Hooke's law (GHL). In other words, a material's stress and strain are proportional within the elastic limit, and the proportionality factor is the material's elastic modulus. The GHL can be used to compute the stress components of each layer in the FG-GPLRC. Subsequently, the study constructs the DE of motion of the FG-GPLRC based on HP, as shown in Equation (12) [22].

$$\begin{cases} \int_{t_1}^{t_2}(\delta T - \delta U - \delta W)dt = 0 \\ \delta T = \int_V \sum_{k=1}^{N} \int_{Z_k}^{Z_{k+1}} \left(\frac{\partial^2 u'}{\partial t^2} + \frac{\partial^2 v'}{\partial t^2} + \frac{\partial^2 w'}{\partial t^2}\right)dXdYdZ \\ \delta U = \int_V \sum_{k=1}^{N} \int_{Z_k}^{Z_{k+1}} \left(\sigma_{ij}^k \delta \varepsilon_{ij}^k\right)dXdYdZ, (i,j = X,Y,Z) \\ \delta W = \int_V \sum_{k=1}^{N} \int_{Z_k}^{Z_{k+1}} \delta\left(k_0 w' - k_1\left(\frac{\partial^2}{\partial X^2} + \frac{\partial^2}{\partial Y^2}\right)w'\right)dXdYdZ \end{cases} \tag{12}$$

In Equation (12), δT denotes the variational component of the kinetic energy of the system. δU denotes the variational component of the strain energy. δW is the variation of the virtual work of the external force. The boundary conditions for the FG-GPLRC on the EF are taken for four-sided simple supported as shown in Equation (13).

$$F_{xx} = M_{xx} = w_b = w_s = 0, (x, y = 0, a) \tag{13}$$

The bending problem of a thin rectangular plate that is simply supported on all sides under multiple loads can be solved using the Navier solution. According to the Navier solution method, the displacement solution for the FV of the FG-GPLRC can be obtained as shown in Equation (14) [27].

$$\begin{cases} u_0(X,Y,t) = \sum_{m=1}^{\infty} \sum_{n=1}^{\infty} \cos\left(\frac{m\pi}{a}X\right)\sin\left(\frac{n\pi}{b}Y\right) \\ v_0(X,Y,t) = \sum_{m=1}^{\infty} \sum_{n=1}^{\infty} v_1 e^{i\mathcal{X}t}\sin\left(\frac{m\pi}{L}X\right)\cos\left(\frac{n\pi}{b}Y\right) \\ w_b(X,Y,t) = \sum_{m=1}^{\infty} \sum_{n=1}^{\infty} w_{b1} e^{i\mathcal{X}t}\sin\left(\frac{m\pi}{L}X\right)\sin\left(\frac{n\pi}{b}Y\right) \\ w_s(X,Y,t) = \sum_{m=1}^{\infty} \sum_{n=1}^{\infty} w_{s1} e^{i\mathcal{X}t}\sin\left(\frac{m\pi}{L}X\right)\sin\left(\frac{n\pi}{b}Y\right) \end{cases} \tag{14}$$

In Equation (14), u_1, v_1, w_{b1}, and w_{s1} are the amplitude in each displacement direction. $i = \sqrt{-1}$, $\mathcal{X}$ is the intrinsic frequency at FV state. m denotes the number of half-waves in the X direction and n denotes the number of half-waves in the Y direction. L represents the length of the plate substituting the FV displacement solution of the FG-GPLRC into the DE of motion, the equation of the intrinsic frequency of the FG-GPLRC in the FV state can be obtained, as shown in Equation (15) [28].

$$|[H] - \mathcal{X}^2[m]| = 0 \tag{15}$$

In Equation (15), $[H]$ denotes the stiffness matrix and $[m]$ denotes the mass matrix. The free vibration natural frequency of FG-GPLRC can be obtained from Equation (15), which forms the basis for evaluating the

dynamic performance of the material and is crucial for understanding the response of composite structures under free vibration. However, to universally compare the effects of different distribution patterns and elastic foundation parameters, the original natural frequencies are nondimensionalized in the results analysis to obtain dimensionless natural frequencies. By solving Equation (15), a series of eigenvalues is obtained, where the square root of each positive real eigenvalue corresponds to a natural frequency. In typical plate vibration analysis, the first four natural frequencies are the most critical, as they jointly determine the fundamental dynamic characteristics of the structure in the free-vibration state. The stiffness and mass matrices are global matrices derived from the motion DE of the FG-GPLRC. Their specific forms depend on the material properties, geometric parameters, and boundary conditions. The stiffness matrix reflects the overall stiffness characteristics of the structure, including the influence of the EF, while the mass matrix represents the inertia distribution of the structure.

3. Results

To investigate how different graphene block distribution modes, affect the vibration characteristics of the FG-GPLRC, the DEs of motion are established. The nonlinear mechanical and FV behaviors of the FG-GPLRC are then analyzed in depth to better understand its vibration and mechanical characteristics.

3.1. Nonlinear Mechanical Analysis Results of FG-GPLRC

In nonlinear vibration analysis, the resonance peak (RP) refers to the frequency at which the response amplitude of the system reaches a local maximum under periodic excitation. The first RP corresponds to the structure's lowest natural frequency (first mode), while the second peak corresponds to its second lowest frequency (second mode), which is usually caused by more complex deformation modes. In the study, graphene is used as the reinforcement and polymer epoxy resin is used as the substrate, and the length, width, and height of FG-GPLRC are 1 m, 1 m, and 0.05 m, respectively, and the number of layers is 10. The graphene sheet has a density of 1.06 g/cm^3, a YM of 1.01 TPa, and a total MF of 1 %. The density of FG-GPLRC is 1.2 g/cm^3 and YM is 3 GPa. The variation of the RP of the first two orders of modes for the upscaled sweep excitation is shown in Figure 6.
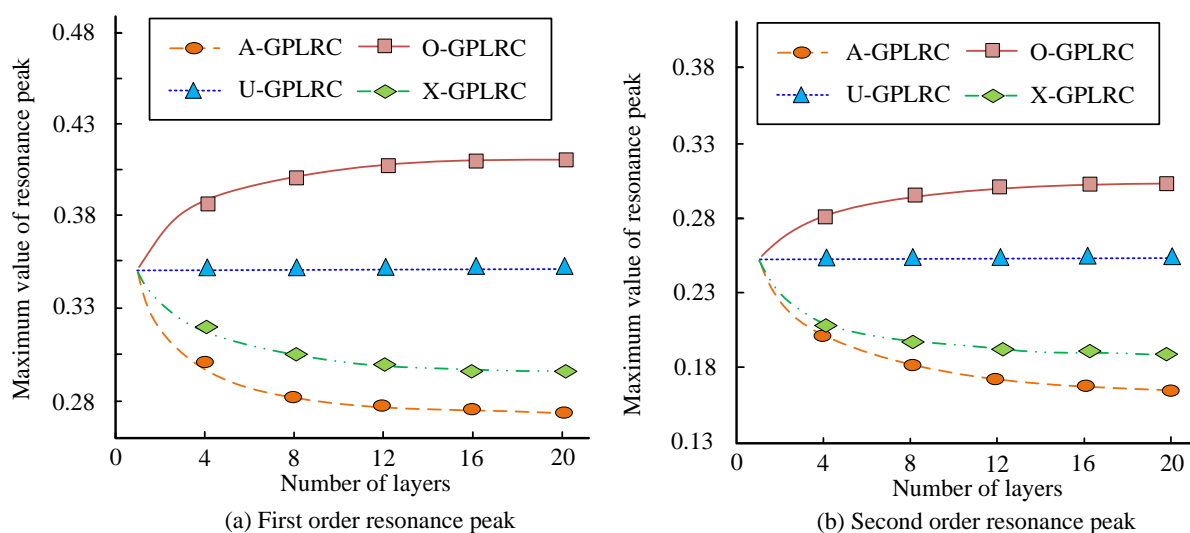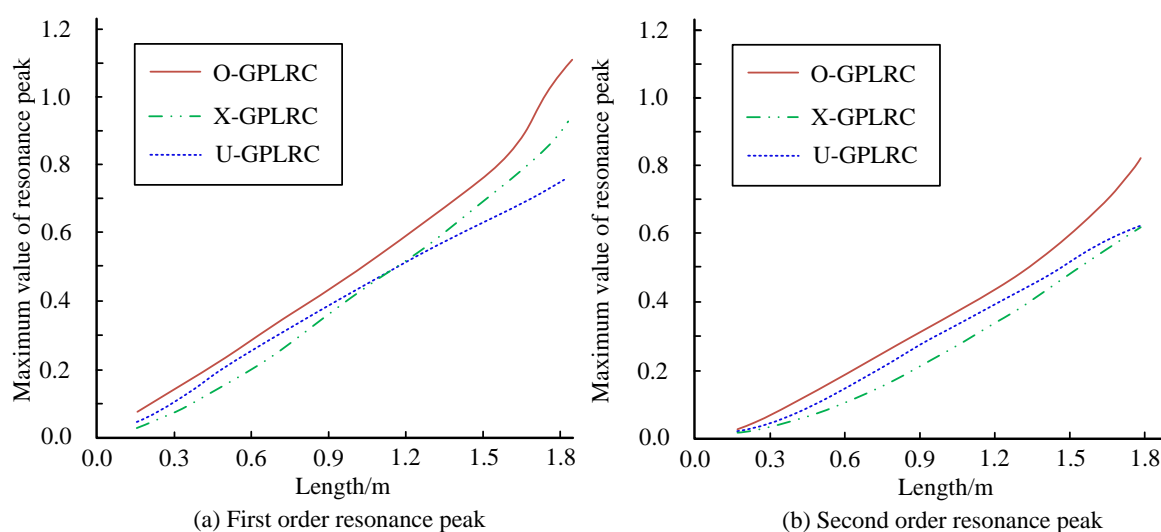

Figure 6. Changes in RPs of the first two modes excited by frequency up sweep excitation.

The first-order RP of the O-GPLRC progressively increases as the number of layers grows, as shown in Figure 6(a). When the number of layers reaches 20, it attains a value of 0.41. The first-order RPs of the A-GPLRC and X-GPLRC gradually decrease. At 20 layers, their RPs are 0.27 and 0.30, respectively. The first-order RP of the U-GPLRC does not show any significant change and remains stable at approximately 0.35.

As the number of layers increases, the patterns of the second-order RPs of the A-GPLRC, O-GPLRC, U-GPLRC, and X-GPLRC follow the same trends as the first-order RPs, as shown in Figure 6(b). However, the overall second-order RPs are all lower than the first-order values, with the second-order RP of the A-GPLRC remaining the lowest at 0.17 when the number of layers is 20.

This behavior arises because, in the O-GPLRC distribution pattern, graphene is mainly concentrated in the middle layer. Increasing the total number of layers makes the core region relatively thicker, which enhances the overall bending stiffness and amplifies the resonance response. In contrast, the A-GPLRC and X-GPLRC distribution modes contain higher graphene concentrations near the surface layers. As the number of layers increases, this results in an average high-stiffness surface-layer effect. Although the overall stiffness increases, the damping characteristics also change, leading to a weakened resonance response. Due to its uniform distribution, the RP of the U-GPLRC remains stable. Therefore, the subsequent analysis focuses only on three distribution patterns: O-GPLRC, U-GPLRC, and X-GPLRC. The variation of the RP under different FG-GPLRC lengths is shown in Figure 7.

(a) First order resonance peak   (b) Second order resonance peak

Figure 7. Changes in RPs of the first two modes under different FG-GPLRC lengths.

In Figure 7(a), the first-order RPs in all three distribution modes gradually increase as the FG-GPLRC length increases. Among them, the first-order RP of O-GPLRC is the highest, reaching 1.11 when the length is 1.8 m. The first-order RP of the X-GPLRC is initially lower than that of the U-GPLRC, but becomes higher once the length exceeds 1.5 m. When the length is 1.8 m, the first-order RP of the U-GPLRC is 0.75. The intersection of the X-GPLRC and U-GPLRC curves occurs because the two distribution patterns exhibit different sensitivities to changes in the structural length. For shorter lengths, the overall stiffness of the U-GPLRC is comparable to or slightly higher than that of the X-GPLRC. However, when the length exceeds a critical value of approximately 1.5 m, the surface-enhancement effect in the X-GPLRC becomes more pronounced. This leads to a higher RP than that of the U-GPLRC, resulting in the intersection observed in the graph. This crossover behavior reflects the dependence of different gradient distribution patterns on structural size.

In Figure 7(b), as the length of the FG-GPLRC increases, the second-order RPs for all three distribution modes also increase, although the rate of increase is lower than that observed for the first-order RPs. The second-order RP of the O-GPLRC remains the highest, reaching 0.83 when the length is 1.8 m. These results indicate that longer FG-GPLRC structures are more prone to vibration and exhibit reduced mechanical performance. Figure 8 shows how the RP of the FG-GPLRC varies under different MFs.
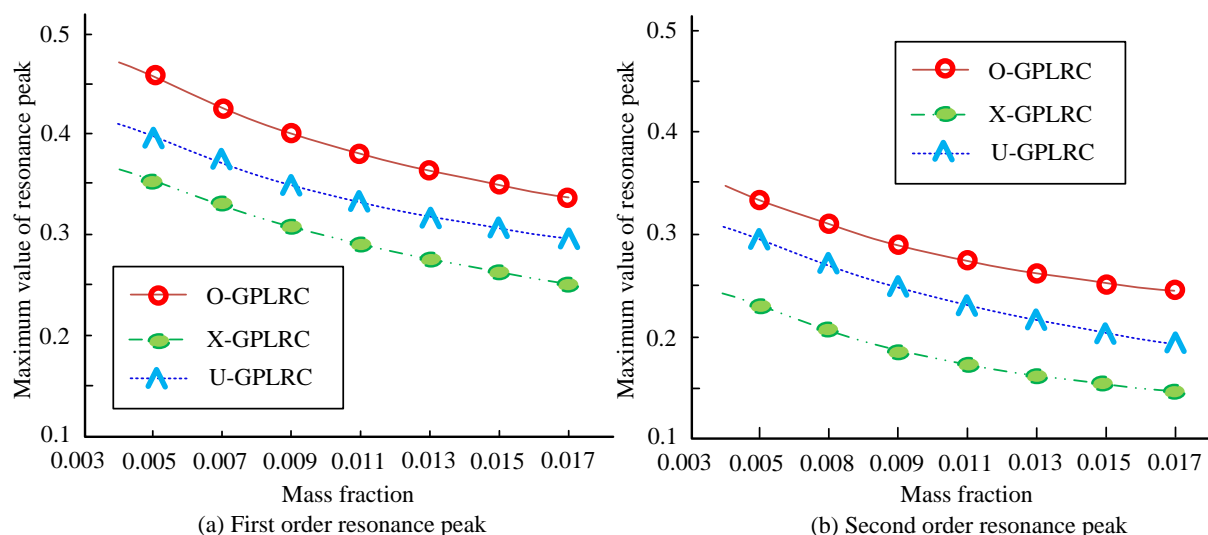
Figure 8. Changes in RPs of FG-GPLRC at different mass fractions.

As the MF increases, the first-order RPs of the three FG-GPLRC distribution patterns progressively decline, as shown in Figure 8(a). This is because increasing the graphene MF significantly enhances the material's overall stiffness, thereby suppressing the vibration response amplitude. Among them, the first-order RP of the O-GPLRC is the highest. When the MF is 0.017, the RP is 0.34. The first-order RP of the X-GPLRC is the lowest; when the MF is 0.018, the RP is 0.25. This trend is consistent with the findings of Merzouki et al. [6], indicating that the gradient distribution of the reinforcing phase has a decisive impact on the dynamic behavior of the structure.

In Figure 8(b), the second-order RPs in all three distribution modes also gradually decrease with increasing MF. Moreover, the second-order RPs are lower than the first-order RPs. The second-order RP of the O-GPLRC remains the highest; when the MF is 0.017, the RP is 0.25. These results show that appropriately increasing the graphene MF in FG-GPLRC can effectively suppress vibration and improve mechanical performance.

When a half-sine pulse with an amplitude of 1 is applied to the FG-GPLRC in different distribution modes, the variation of the RP for different numbers of layers and MFs is shown in Figure 9.
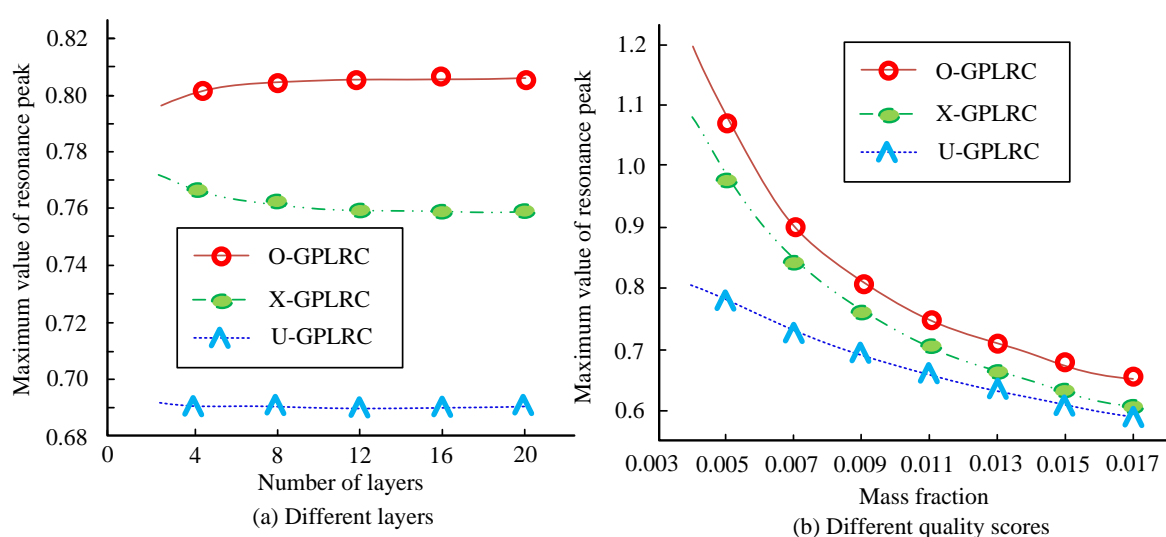

Figure 9. Changes in RPs under different layers and mass fractions.

The RP of the O-GPLRC progressively increases as the number of layers grows, as shown in Figure 9(a). The RP of the X-GPLRC gradually decreases, while the RP of the U-GPLRC shows no significant change and stabilizes around 0.69. In Figure 9(b), the RPs in all three distribution modes decrease as the MF increases. Among them, the RP of the O-GPLRC is the highest; when the MF is 0.017, the RP reaches 0.59. This result further confirms that adjusting the gradient distribution and graphene content effectively controls the impact resistance of composite materials. This finding is consistent with the "stiffness designability" observed by Zhao et al. [8] in functionally graded rotating structures.

### 3.2. FV Analysis Results of FG-GPLRC

The variation of FG-GPLRC non-dimensional natural frequency (NDNF) at different values of k_0 and k_1 is shown in Figure 10.
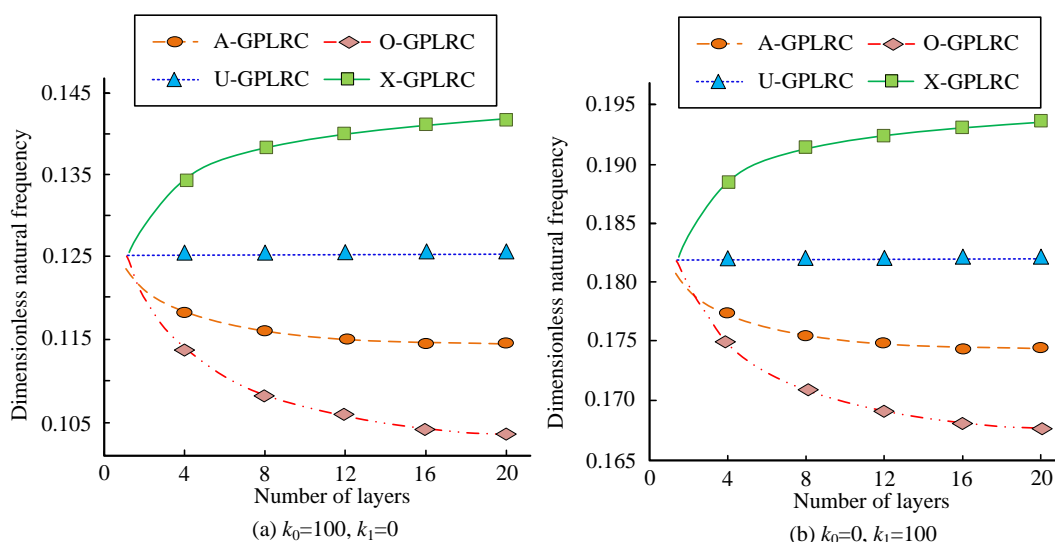
Figure 10. Variation of non-dimensional natural frequency of FG-GPLRC.

In Figure 10(a), when $k_0 = 100$, the NDNF of X-GPLRC gradually increases as the number of the layers increases. When the number of layers reaches 20, the NDNF is 0.142. The NDNF of the U-GPLRC does not change with the number of layers. As the number of layers increases, the NDNF of the A-GPLRC and O-GPLRC steadily decreases, and when the number of layers is 20, the NDNF values is 0.115 and 0.103, respectively. In Figure 10(b), the trend of the NDNF of the four distribution patterns when $k_1 = 100$ is consistent with the trend observed when $k_0 = 100$. However, the overall NDNF values are higher. These results suggest that increasing the number of layers can appropriately improve the intrinsic frequency of the FG-GPLRC.

The variation of the NDNF of FG-GPLRC under different elastic foundations (EFs) with different aspect ratios (ARs) is shown in Figure 11.
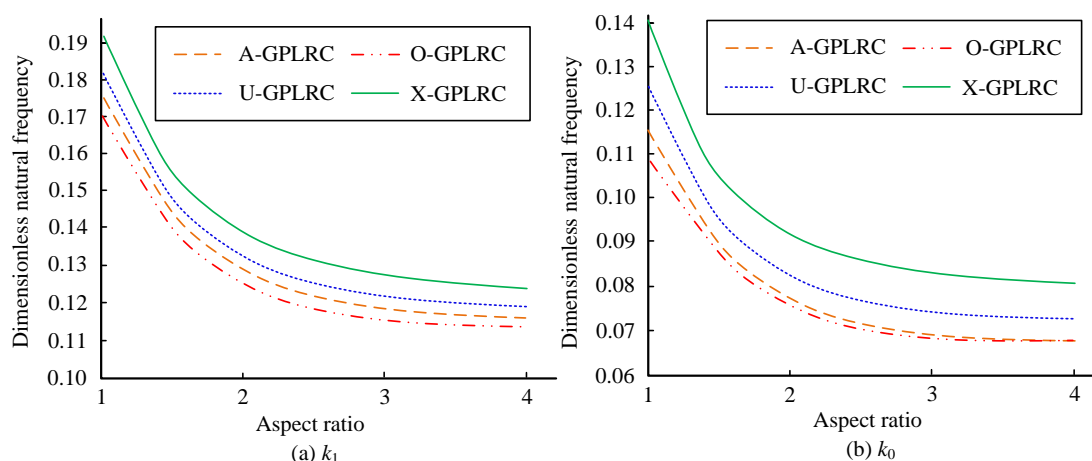
Figure 11. Variation of the non-dimensional natural frequency under different EFs

In Figure 11(a), for all four distribution patterns, the NDNF of the FG-GPLRC under the Winkler EF progressively decreases as the AR increases. Among them, the NDNF of the X-GPLRC is the highest; when the AR is 4, the NDNF is approximately 0.124. This behavior is mainly attributed to the high graphene content near the surface layers of the X-GPLRC, which effectively enhances the bending stiffness. This result is consistent with the findings of Gao et al. [7]. Their study also showed that a surface-enhanced gradient mode can more effectively influence the displacement distribution and the overall stiffness of the structure.

In Figure 11(b), under the Pasternak EF, the NDNF of the FG-GPLRC in all four distribution patterns also gradually decreases as the AR increases. Furthermore, once the AR exceeds 2, its influence on the NDNF becomes progressively weaker.

To further examine the effect of different matrix materials on the characteristics of the FG-GPLRC, the study uses the X-GPLRC as an example and considers epoxy resin, aluminum alloy, and titanium alloy as matrix materials. The corresponding Poisson's ratios are 0.35, 0.31, and 0.35; the densities are 1210 kg/m³, 2690 kg/m³, and 4500 kg/m³; and the Young's moduli are 3 GPa, 70 GPa, and 100 GPa, respectively. Figure 12 illustrates how the inherent frequencies of the FG-GPLRC vary with different matrix materials.
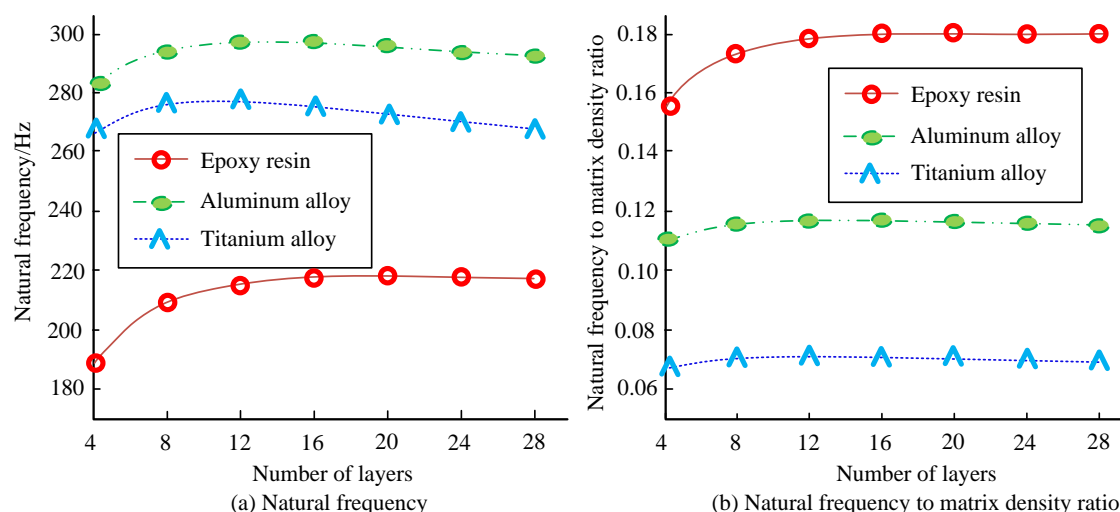
Figure 12. Natural frequencies of the FG-GPLRC under different matrix materials.

In Figure 12(a), as the number of layers increases, the intrinsic frequency of the FG-GPLRC with titanium and aluminum alloy matrices first increases and then decreases. The intrinsic frequency of the FG-GPLRC with an epoxy resin matrix is the lowest among the three. In Figure 12(b), the ratio of the intrinsic frequency to the density of the matrix is the highest for epoxy resin, reaching approximately 0.17. These results indicate that although a metal matrix can provide higher absolute stiffness, an epoxy resin matrix offers greater advantages for achieving lightweight design. Such a design can significantly reduce structural weight while maintaining acceptable frequency performance.

4. Discussion and Conclusion

To investigate the distributional effects of the FG-GPLRC, this study established the DEs for motion control based on the HTMM and HP, and analyzed both the nonlinear and FV behaviors of the FG-GPLRC. The results indicate that gradient distribution patterns such as the O-GPLRC and X-GPLRC can significantly regulate the vibration response and natural frequencies of the structure, performing better than the uniform distribution (U-GPLRC). In addition, increasing the MF of graphene effectively enhances the material's stiffness and suppresses vibration, whereas increasing the structural size reduces dynamic stability. Among the results, the second-order RP of the O-GPLRC was the highest, reaching 0.25 when the MF was 0.017. As the number of layers increases, the resonance peak of the uniform distribution mode remains unchanged and stabilizes at approximately 0.69. The ratio of intrinsic frequency to matrix density is the highest for the epoxy resin matrix, at about 0.17.

In summary, different graphene block distribution patterns exhibit varying effects on the mechanical enhancement of the FG-GPLRC. A reasonable increase in the graphene MF can effectively improve these properties. However, this study focuses solely on the nonlinear and FV behaviors of the FG-GPLRC. Other mechanical behaviors, such as bending under thermal environments, should be examined in future.

References

[1] Y. Elmoghazy, E. M. O. Abuelgasim, S. A. Osman, Y. R. H. Afaneh, O. M. A. Eissa, and B. Safaei,"Effective mechanical properties evaluation of unidirectional and bidirectional composites using virtual domain approach at microscale,"*Archives of Advanced Engineering Science*, vol. 46, no. 6, pp. 786-794, 2023, https://doi.org/10.47852/bonviewAAES32021723

[2] F. Hou, S. Wu, Z. Moradi, and N.Shafiei,"The computational modeling for the static analysis of axially functionally graded micro-cylindrical imperfect beam applying the computer simulation,"*Engineering with Computers*, vol. 38, no. 4, pp. 3217-3235, 2022, https://doi.org/10.1007/s00366-021-01456-x

[3] B. M. Cuong, A. Tounsi, N. T. H. Van, and P.Van Minh,"Finite element modelling for the static bending response of rotating FG-GPLRC beams with geometrical imperfections in thermal mediums,"*Computers and Concrete*, vol. 33, no. 1, pp. 91-102, 2024, https://doi.org/10.12989/cac.2024.33.1.091

[4] K. Duan, Z. Li, J. Chen, L. Li, Y. Hu, Y. Zhang, J. W. Zhang, and Y. Lu,"Gradient evolution in graphene reinforced carbon/carbon composites,"*Carbon*, vol. 206, no. 2, pp. 295-302, 2023, https://doi.org/10.1016/j.carbon.2023.02.056

[5] B. Zheng, Z. Zheng, and G. X.Gu,"Designing mechanically tough graphene oxide materials using deep reinforcement learning,"*npj Computational Materials*, vol. 8, no. 1, pp. 2139-2147, 2022, https://doi.org/10.1038/s41524-022-00919-z

[6] T. Merzouki, H. M. S. Ahmed, A. Bessaim, M. Haboussi, R. Dimitri, and F.Tornabene,"Bending analysis of functionally graded porous nanocomposite beams based on a non-local strain gradient theory,"*Mathematics and Mechanics of Solids*, vol. 27, no. 1, pp. 66-92, 2022, https://doi.org/ 10.1177/10812865211011759

[7] X. Gao, Z. Wang, and L.Ma,"Bending and buckling analysis of functionally graded graphene platelets reinforced composite plates supported by local elastic foundations based on simple refined plate theory,"*Archive of Applied Mechanics*, vol. 94, no. 8, pp. 2123-2150, 2024, https://doi.org/10.1007/s00419-024-02629-y

[8] T. Zhao, Y. Cui, Y. Wang, and H.Pan,"Vibration characteristics of graphene nanoplatelet reinforced disk-shaft rotor with eccentric mass,"*Mechanics of Advanced Materials and Structures*, vol. 29, no. 24, pp. 3485-3498, 2022, https://doi.org/10.1080/15376494.2021.1904525

[9]   J. Adhikari, R. Kumar, and S. C.Jain,"Using modified Halpin Tsai based approach for electromechanical analysis of functionally graded graphene reinforced piezoelectric tile,"*International Journal of Mechanics and Materials in Design*, vol. 19, no. 2, pp. 299-318, 2023, https://doi.org/10.1007/s10999-022-09632-7

[10]   Q. Cao, S. Goswami, and G. E.Karniadakis,"Laplace neural operator for solving differential equations,"*Nature Machine Intelligence*, vol. 6, no. 6, pp. 631-640, 2024, https://doi.org/10.1038/s42256-024-00844-4

[11]   S. Tang, X. Feng, W. Wu, and H. Xu,"Physics-informed neural networks combined with polynomial interpolation to solve nonlinear partial differential equations,"*Computers & Mathematics with Applications*, vol. 132, no. 12, pp. 48-62, 2023, https://doi.org/10.1016/j.camwa.2022.12.008

[12]   I. Barbaros, Y. Yang, B. Safaei, Z. Yang, Z. Qin, and M.Asmael,"State-of-the-art review of fabrication, application, and mechanical properties of functionally graded porous nanocomposite materials,"*Nanotechnology Reviews*, vol. 11, no. 1, pp. 321-371, 2022, https://doi.org/10.1515/ntrev-2022-00

[13]   M. Nadeem and J. H.He,"The homotopy perturbation method for fractional differential equations: Part 2, two-scale transform,"*International Journal of Numerical Methods for Heat & Fluid Flow*, vol. 32, no. 2, pp. 559-567, 2022, https://doi.org/10.1108/HFF-01-2021-0030

[14]   Y. Kai, S. Chen, K. Zhang, and Z.Yin,"Exact solutions and dynamic properties of a nonlinear fourth-order time-fractional partial differential equation,"*Waves in Random and Complex Media*, vol. 35, no. 2, pp. 2539-2550, 2025, https://doi.org/10.1080/17455030.2022.2044541

[15]   Y. Wang, Y. Zhou, C. Feng, J. Yang, D. Zhou, and S.Wang,"Numerical analysis on stability of functionally graded graphene platelets (GPLs) reinforced dielectric composite plate,"*Applied Mathematical Modelling*, vol. 101, no. 8, pp. 239-258, 2022, https://doi.org/10.1016/j.apm.2021.08.003

[16]   A. Yusuf, M. M. Bhatti, and C. M.Khalique,"Computational study of the thermophysical properties of graphene oxide/vacuum residue nanofluids for enhanced oil recovery,"*Journal of Thermal Analysis and Calorimetry*, vol. 150, no. 1, pp. 771-783, 2025, https://doi.org/10.1007/s10973-024-13921-y

[17]   H. Hardani, M. Afshari, M. R. Samadi, H. Afshari, and S. A.López,"An enhancement in the tensile modulus and bending resistance of polylactic acid/carbon nanotube composite by optimizing FFF process parameters,"*Journal of Thermoplastic Composite Materials*, vol. 38, no. 4, pp. 1379-1403, 2025, https://doi.org/10.1177/08927057241268831

[18]   S. Ghasemi, A. Espahbodi, N. Gharib, Y. Zare, and K. Y.Rhee,"Prediction of interphase parameters for nanocellulose composites using a modified Halpin–Tsai approach,"*Cellulose*, vol. 30, no. 15, pp. 9439-9452, 2023, https://doi.org/10.1007/s10570-023-05445-9

[19]   Z. Yang, T. Yin, Y. Wu, D. Zhuang, J. Yin, and J.Ma, "Mixed-mode I/II fracture properties and failure characteristics of microwave-irradiated basalt: An experimental study,"*Fatigue & Fracture of Engineering Materials & Structures*, vol. 46, no. 3, pp. 814-834, 2023, https://doi.org/10.1111/ffe.13897

[20]   S. Al-Houri, M. A. Al-Osta, Q. Gawah, F. Bourada, A. Tounsi, S. U. Al-Dulaijan, and A.Tounsi, "Wave propagation analysis of composite beams reinforced with nonlinear FG-CNT distributions supported on Kerr elastic foundation utilizing an improved integral first-order shear deformation theory,"*Geomechanics and Engineering*, vol. 39, no. 5, pp. 483-501, 2024, https://doi.org/10.12989/gae.2024.39.5.483

[21]   H. Bagheri, Y. Kiani, and M. R.Eslami,"Geometrically nonlinear response of FGM beams on elastic foundation subjected to thermal shock,"*Iranian Journal of Science and Technology, Transactions of Mechanical Engineering*, vol. 47, no. 1, pp. 187-201, 2023, https://doi.org/10.1007/s40997-022-00506-z

[22]   H. Ma,"Simplified Hamiltonian-based frequency-amplitude formulation for nonlinear vibration systems,"*Facta Universitatis, Series: Mechanical Engineering*, vol. 20, no. 2, pp. 445-455, 2022, https://doi.org/10.22190/FUME220420023M

[23]   J. Dong, L. Wang, L. Shi, and X.Wu,"Multi physical field coupling analysis of freeze thaw effect on permafrost slope supported by new frame ventilation anchor,"*Journal of Basic Science and Engineering*, vol. 33, no. 2, pp. 436-451, 2025, https://doi.org/10.16058/j.issn.1005-0930.2025.02.012

[24]   F. P. Soffietti, D. F. Turello, and F.Pinto,"Pseudo-static Winkler springs for longitudinal underground structures subjected to shear waves,"*Geomechanics and Geoengineering*, vol. 19, no. 6, pp. 1075-1096, 2024, https://doi.org/10.1080/17486025.2024.2343355

[25]　T. Z. Ma, J. B. Hao, C. D. Sun, and Z. Z. Wang,"Bearing capacity analysis of pile foundations under composite loads based on the pasternak foundation model under small deformation,"*Soil Mechanics and Foundation Engineering*, vol. 61, no. 5, pp. 436-444, 2024, https://doi.org/10.1007/s11204-024-09994-4

[26]　S. M. Shiyekar and T. Kant,"A study on anisotropic behavior of functionally graded plates by higher order refined theory,"*Mechanics of Advanced Materials and Structures*, vol. 31, no. 27, pp. 9166-9178, 2024, https://doi.org/10.1080/15376494.2023.2266825

[27]　T. V. Vu, H. L. Cao, G. T. Truong, and C. S. Kim,"Buckling analysis of the porous sandwich functionally graded plates resting on Pasternak foundations by Navier solution combined with a new refined quasi-3D hyperbolic shear deformation theory,"*Mechanics Based Design of Structures and Machines*, vol. 51, no. 11, pp. 6227-6253, 2023, https://doi.org/10.1080/15397734.2022.2038618

[28]　M. Haskul, and M. Kisa,"Free-vibration analysis of cracked beam with constant width and linearly varying thickness,"*Emerging Materials Research*, vol. 11, no. 1, pp. 125-137, 2022, https://doi.org/10.1680/jemmr.21.00015a

　　　　　　　　　　　　　　　　　　　　　　https://doi.org/10.64486/m.65.2.8